Turkish Journal of Earth Sciences

Volume 30 | Number 2 Article 5

1-1-2021

Time-dependent model for earthquake occurrence and effects of design spectra onstructural performance: a case study from the North Anatolian Fault Zone, Turkey

ERCAN IŞIK

YUNUS LEVENT EKİNCİ

NİLGÜN LÜTFİYE SAYIL

AYDIN BÜYÜKSARAÇ

MEHMET CİHAN AYDIN

TÜBİTAK

Turkish Journal of Earth Sciences

http://journals.tubitak.gov.tr/earth/

Research Article

Turkish J Earth Sci
(2021) 30: 215-234

doi:10.3906/yer-2004-20

Time-dependent model for earthquake occurrence and effects of design spectra on structural performance: a case study from the North Anatolian Fault Zone, Turkey

Ercan IŞIK[1], Yunus Levent EKİNCİ[2,3], Nilgün SAYIL[4], Aydın BÜYÜKSARAÇ[5,*], Mehmet Cihan AYDIN[1]

[1]Department of Civil Engineering, Bitlis Eren University, Bitlis, Turkey
[2]Department of Archaeology, Bitlis Eren University, Bitlis, Turkey
[3]Career Application and Research Centre, Bitlis Eren University, Bitlis, Turkey
[4]Department of Geophysical Engineering, Karadeniz Technical University, Trabzon, Turkey
[5]Çan Vocational School, Çanakkale Onsekiz Mart University, Çanakkale, Turkey

Received: 24.04.2020 • **Accepted/Published Online:** 21.12.2020 • **Final Version:** 22.03.2021

Abstract: We have investigated the time-dependent seismicity model of the earthquake occurrence on a regional basis through the North Anatolian Fault Zone (NAFZ). To that end, the studied region has been subdivided into 7 seismogenic zones considering the seismotectonic criteria, and then regional time and magnitude predictable (RTIMAP) model has been performed. Intervened times and magnitudes of main shocks produced in each zone have predictive properties defined by the RTIMAP. The probabilities of the next main shocks in 5 decades and the magnitudes of the next events have been estimated using the formation time and magnitude of the past events in the zones. In the second step of the study, we have considered 17 settlements located on the NAFZ to perform point-based site-specific seismic hazard analyses and to determine the design spectra and earthquake parameters using updated Turkish Earthquake Hazard Map. Eigen value and static adaptive pushover analyses have been applied for the sample reinforced concrete building using the design spectra obtained from each settlement. This sample building has been modelled with the same structural characteristics (i.e. material strength, column and beams, applied loads, etc.) for all of the settlements. We have determined that the earthquake building parameters differ from each other which indicates the significance of site-specific seismicity characteristics on the building performance.

Key words: North Anatolian Fault Zone, seismic hazard, earthquake prediction, time-dependent model, site-specific spectra, adaptive static analysis

1. Introduction

Turkey has experienced many destructive earthquakes in both instrumental and historical periods. Earthquake hazard potential determination and earthquake prediction studies are of great importance to minimize the loss of life and properties. Herein we performed regional and time-based analyses of seismicity to reveal the earthquake potential along the North Anatolian Fault Zone (NAFZ). Time-dependent models are widely used in seismic hazard studies (e.g., Cornell, 1968; Caputo, 1974; Papadopoulos and Voidomatis, 1987). Gutenberg–Richter approach is commonly used for these time-dependent models. Due to some constraints and the shortcomings of independent models, several approaches have been developed to produce time-dependent models (e.g., Papazachos, 1992; Stein et al., 1997; Parsons et al., 2000; Mulargia and Geller, 2003; Coral, 2006; Shanker et al., 2012). These approaches indicate that the time of repetition for earthquakes occurring at the edge of a fault supports time predictive models. In these models, the rate of the slip of previous earthquake is proportional to the time interval between two major earthquakes occurred on the same location. Additionally, when the stress reaches a limit value a major earthquake occurs. Based on historical and instrumental seismological events and geological observations it is mentioned that strong ($M_s \geq 6.0$) and large ($M_s \geq 7.0$) earthquakes occur in certain seismogenic regions and follow the relations of the regional time and magnitude predictable (RTIMAP) model (Papazachos et al., 2014). The magnitude predictable models show the relationship between the past and next earthquakes magnitudes. Hence, time and magnitude predictable models are characterized using RTIMAP model (Papazachos, 1992). There have been many studies performed for different seismogenic regions using this approach (e.g., Mogi, 1985; Shanker, 1990; Paudyal et al., 2008; Shanker et al., 2012; Papazachos et al., 2014, 2016).

* Correspondence: absarac@comu.edu.tr

Major losses of life and property due to the destructive earthquakes have pioneered the development of the earthquake resistant building design principles. Every earthquake occurrence is considered to be a realistic and reliable test for buildings. Earthquake codes need to be updated partly or completely based on the new knowledge obtained from the significant earthquakes and technological developments. Thus, many changes have been made in Turkey to date and the recently updated Turkish Seismic Codes (2019) is a notable example of these renewal and modifications. In particular, the losses occurred due to the Van earthquakes (2011) showed the necessity of the update. Seismicity parameters of the region are among the most important data in structural analyses under earthquake loads. The accurate determination of these parameters directly affects the performance of the structures during an earthquake. The recently updated seismic code provided important changes in terms of earthquake structure relationship. Earthquake design spectra can be obtained for any specific location through the new codes and the seismic hazard map. In the previous codes, some significant factors were being ignored while evaluating with a regional basis. Briefly, nowadays point-based site-specific analyses began to be used instead of regional basis macrozoning analyses. Using the revised Turkish Seismic Hazard Map in the analyses became obligatory based on the newly updated code. Hence, Turkish Earthquake Hazard Map Interactive Web Application (TEHMIWA) has been launched to perform earthquake building parameters for any specific location since 2019 (TBEC-2018)[1].

Earthquake parameters are directly linked to seismicity characteristics of the region where the building will be built. One of the seismicity characteristics is the presence of faults located in the region. In this paper, firstly we used the time-dependent seismicity model for earthquake generation for 7 defined seismogenic zones through the NAFZ. By this way, the magnitude predictable models showing the relationship between the past and next earthquakes magnitudes were estimated on a regional basis. Then, the required earthquake parameters for the structural analysis were obtained using geographic location, local ground classes and earthquake ground motion level determined from TEHMIWA. Seventeen settlements along to NAFZ were taken into consideration and earthquake parameters were calculated by setting the local soil conditions and earthquake ground motion level constant for each location. Additionally, we obtained structural parameters of the building located on the fault zone using the same seismicity and structural characteristics. Short period mapping, spectral acceleration coefficient, peak ground acceleration (PGA), local ground effect coefficients, design spectral acceleration coefficients and horizontal and vertical elastic spectrum curve were calculated for the settlements. The earthquake ground motion level (DD-2), that is 10% probability of exceedance (repetition period 475 years) in 50 years, and the ground type ZD were used. Structural analyses were performed to sample reinforced concrete (RC) building using the obtained design spectra. Static adaptive pushover analysis was carried out considering local soil conditions. The base shear force, displacement, stiffness and target displacement for performance criteria were calculated for each settlement.

[1] Republic of Turkey Ministry of Interior Disaster and Emergency Management Presidency (2021). Türkiye Deprem Tehlike Haritaları (in Turkish) [online]. Website https://tdth.afad.gov.tr [accessed 08 September 2019].

2. A brief on the NAFZ

The well-known broad arc-shaped dextral strike-slip NAFZ extending for about 1200 km from Karlıova (Bingöl, eastern Turkey) to the Gulf of Saros (Aegean Sea) is an important fault system in the world (Figure 1). Continental collision of Arabian and Eurasian Plates through the Bitlis-Zagros Suture Zone (BZSZ in Figure1) has triggered the formation of this transform fault (Bozkurt, 2001). This fault system has been paid much attention so far due to its noteworthy seismic activities and the role on the tectonics of eastern Mediterranean region (e.g., Ambraseys, 1970; Mc Kenzie, 1972; Dewey, 1976; Şengör, 1979; Şengör et al., 1985, 2014; Barka, 1992; Tatar et al., 1995, 1996, 2012; İşseven and Tüysüz, 2006; Zabcı, 2019). The NAFZ extends in a shear zone reaching up to about 100 km in width (İşseven and Tüysüz, 2006). In the eastern Anatolia NAFZ forms a triple junction links with the East Anatolian Fault Zone (EAFZ) (Bozkurt, 2001). It is one of the major elements controlling the neotectonics of the Anatolian Plate located on the Alpine-Himalayan orogenic belt (Bozkurt, 2001). This continental fault zone, which develops wider westward (Şengör et al., 2005), runs roughly parallel to the Black Sea and also shapes the Anatolian and Eurasian Plates tectonic boundary (Figure 1). The main segments of NAFZ are the 350 km long Erzincan segment, 260 km long Ladik-Tosya segment, 180 km long Gerede segment and >100 km long Saros segment. These main segments were ruptured in 1939, 1943, 1944 and 1912, respectively. The other segments are the Varto segment (ruptured in 1966) and Mudurnu Valley segment (ruptured in 1957 and 1967) which are located at the eastern end and on the branches to the east, respectively. It is now well known that stress transfer can trigger more earthquakes after a major earthquake. NAFZ is a typical example for stress transfer. If the accumulated tectonics stresses are high and close to the collapse threshold, it is believed that a positive Coulomb stress change generally encourages the occurrence of an earthquake on a nearby fault (King et

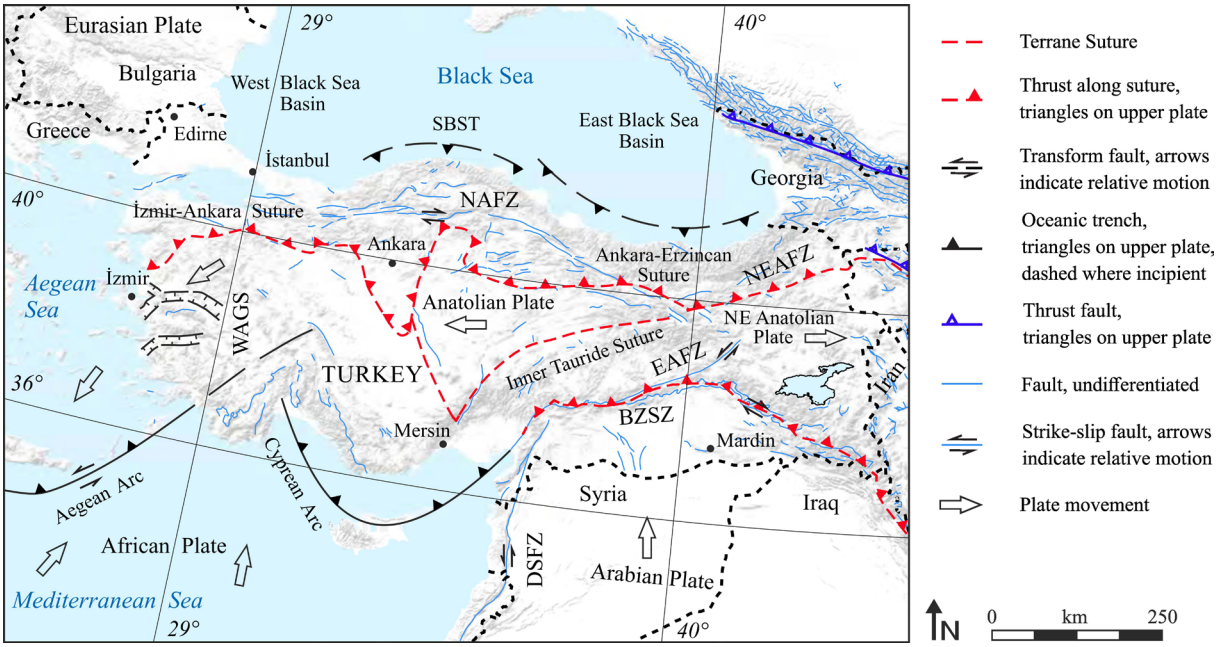

Figure 1. Tectonic map of Turkey and the surrounding (compiled with Okay and Tüysüz, 1999; Yiğitbaş et al., 2004; USGS, 2010; Ekinci et al., 2020, 2021; Işık et al., 2020). NAFZ, North Anatolian Fault Zone; EAFZ, East Anatolian Fault Zone; NEAFZ, Northeast Anatolian Fault Zone; BZSZ, Bitlis-Zagros Suture Zone; DSFZ, Dead Sea Fault Zone; WAGS, West Anatolian Graben System; SBST, Southern Black Sea Thrust.

al., 1994; Harris and Simpson, 1996; Hamling et al., 2014). The static stress transfer model in the eastern part of the NAFZ and the dynamic stress transfer model between the west parallel branches of the NAFZ were revealed by Bektaş et al. (2007), which provides important parameters to predict seismic hazards on the NAFZ. On contrary to the central and eastern parts NAFZ bifurcates to some strands in the Marmara region. Mudurnu Valley segment that was ruptured in 1957 and 1967 is on the branches to the west. İznik-Mekece segments is the southern strand and the Sapanca-İzmit segment which was ruptured in 1953 is the northern strand. Furthermore, the main regions contain some sub regions toward the both directions.

3. Analyses and results

3.1. RTIMAP model

Producing the RTIMAP model consists of a three-step procedure. Firstly, seismogenic zones are selected based on some criteria such as the distribution of the events, seismicity, the largest magnitude earthquakes, fault types, the effects of earthquakes on each other, dimensions of the fractures associated with the magnitude of the earthquakes (Papazachos et al., 1997). The selected zones should include the main fault of the largest event ($Ms \geq 7.0$), and the other faults producing smaller earthquakes. Earthquakes in the selected regions do not have to occur on the same fault, provided that they show the same tectonic properties. Here, we selected 7 seismogenic zones (Figure 2) considering the base and side segments of NAFZ.

Seismogenic zone 1 includes the Çınarcık basin located in the eastern Marmara region. A strike-slip type mechanism is dominant in Northwest part of Çınarcık basin, but a normal faulting mechanism is dominant in its central part. The largest event in this zone is the İzmit earthquake (M_S = 7.8) occurred in 1999. Seismogenic zone 2 covers the right-lateral strike-slip Düzce fault and the largest event in this zone was occurred in Düzce (M_S = 7.5) in 1999. Seismogenic zone 3 includes Tosya, Ilgaz, and Çerkeş intramountain basins. Thrust faults are approximately 30 km long and have an average strike consistent with the dextral slip on the NAFZ (Hubert-Ferrari et al., 2002). The largest events in this zone was occurred in Ilgaz basin (M_S = 7.2, in 1943) and Çerkeş basin (M_S = 7.2, in 1944). Seismogenic zone 4 covers the Havza-Ladik basin. The largest event in this zone was occurred in 1942 (M_S = 7.0). Seismogenic zone 5 includes Erbaa pull-apart basin which is a discontinuity along the fault (Ambraseys, 1970). The largest event in this zone was occurred in 1916 (M_S = 7.1). Seismogenic zone 6 covers the NW-SE striking Erzincan basin which appears to be a major step over along the NAFZ (Şengör, 1979; Hubert-Ferrari et al., 2002). The largest events in this seismogenic

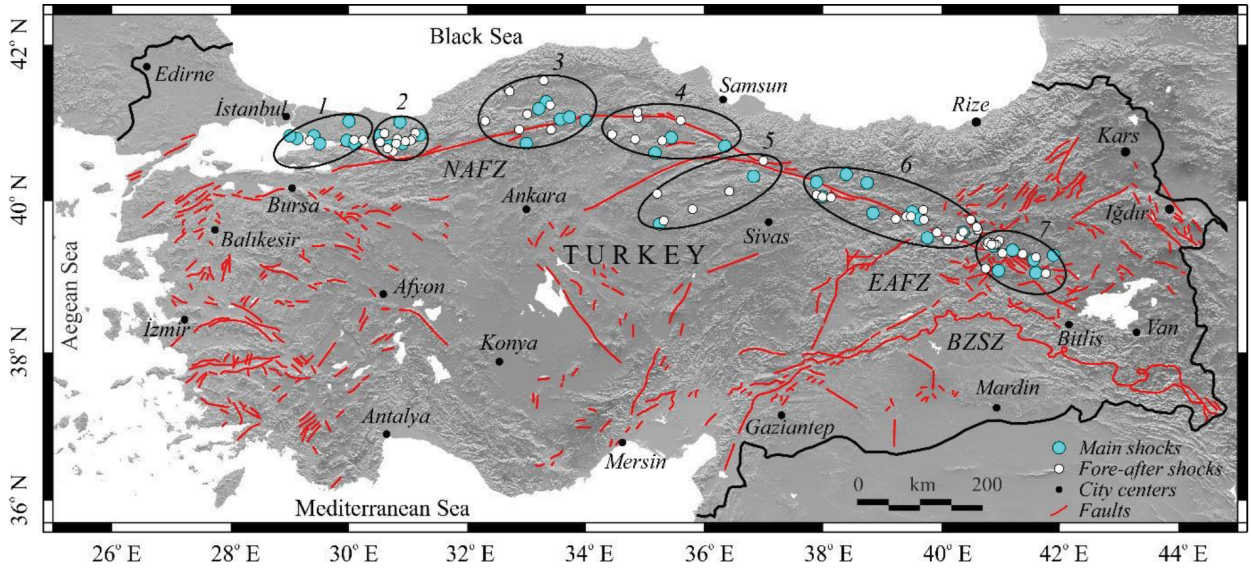

Figure 2. Seven seismogenic zones used in this study. Cyan and white coloured circles show shallow main shocks and previous or after main shocks, respectively.

zone were occurred in 1938 (M_S = 7.9) and in 1949 (M_S = 7.0). Seismogenic zone 7 includes the Karlıova Triple Junction which is related to the continental collision of Arabian and Eurasian Plates. The major event in this zone was occurred in 1966 (M_S = 7.0).

We used instrumental ($M_S \geq 5.5$, until the end of 2019) and historical data with maximum intensities of $I_0 \geq 9.0$ corresponding to surface wave magnitude $M_S \geq 7.0$ (Sayıl, 2013). Different-scaled magnitudes were transformed to M_S using empirical equations obtained from regional earthquakes (Figure 3). The experimental scaling relationship between M_S and I_0 for the study area was calculated according to Sayıl (2014). Determined relationships here are consistent with the earlier studies (e.g. Shebalin et al., 1998; Burton et al., 2004; Bayliss and Burton, 2007; Makropoulos et al., 2012). Completeness of the data is a significant factor in RTIMAP model. Hence, we tested the completeness of the catalogue via the method proposed by Al-Tarazia and Sandvol (2007) by choosing the smallest magnitude i.e. cut-off magnitude (M_c) as 5.5 and 7.0 for instrumental and historical periods, respectively in all seismogenic zones. The data should comprise all the events taken place in a specific seismogenic region during a time interval with magnitudes larger than an exact M_c (Chingtham et al., 2016). The RTIMAP model of seismicity is expressed as follows (Papazachos and Papaioannou, 1993):

$$\log T_t = b\, M_{min} + cM_p + d \log M_0 + q \quad (1)$$

$$M_f = BM_{min} + CM_p + D\log M_0 + m \quad (2)$$

where b, c, d, q, B, C,D and m represent the constant terms, T_t denote the interval time measured in years, M_{min} is the minimum main shock, M_f and M_p denote the magnitudes of following and preceding main shock, respectively, and M_0 represent the yearly seismic moment ratio in the source.

Calculating the seismic moment (M_0) of the selected zones is the second step of the procedure (Molnar, 1979). The largest earthquake (M_{max}) of each zone is determined by considering the available data. For these seismogenic zones, constants a and b' (Gutenberg and Richter, 1944) are normalized for a year. The calculated values of our case are given in Table 1. Since the method is performed to largest shocks of earthquakes clustered in time and space, we performed declustering process at the last step using the expression given below (Papazachos et al., 1997).

$$t_p = 3\ years,\ \log t_a = 0.06 + 0.13\, M_p \quad (3)$$

where t_p and t_a denote the total durations of preshocks and postshocks activities, respectively. Earthquake data set used for RTIMAP model is shown in Table 2.

The model proposed by Papazachos and Papaioannou (1993) was fitted to determine the parameters of Equation 1. We used a multilinear regression approach (Weisberg, 1980) to obtain the constant terms of the Equations 1 and 2. Using M_0 (Table 1) and the observational data listed in Table 2 (T_t, M_{min}, M_p, M_f) we obtained the constant terms in Equation 1 as follows:

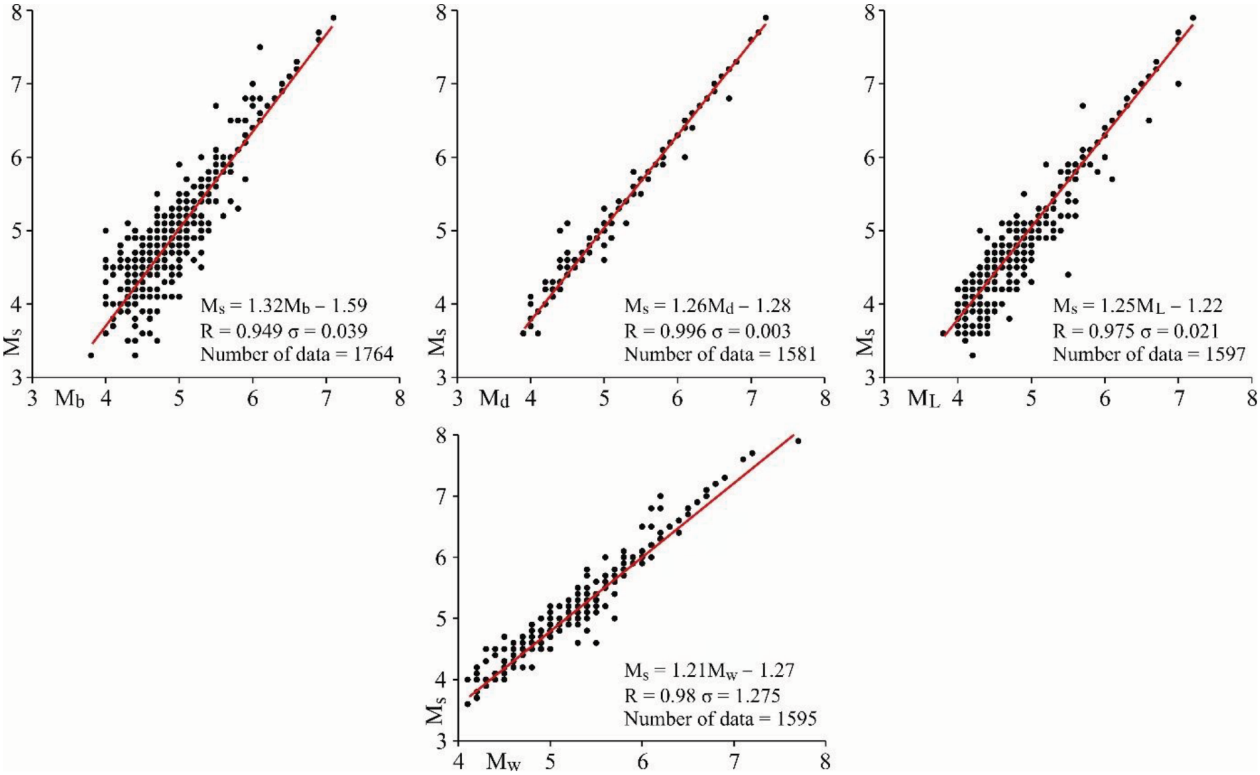

Figure 3. Correlations of M_S – M_b, M_w, M_L and M_d used in this study.

$$\log T_t = 0.16\, M_{min} + 0.16\, M_p - 0.27 \log M_0 + 6.36. \quad (4)$$

The multiple correlation coefficient (R) and standard deviation (σ) of Equation 4 are 0.63 and 0.32, respectively. The relationship with increasing slope between T_t and M_p indicates the validity of the method for the studied area. Similarly, the constant terms in Equation 2 were determined as given below

$$M_f = 0.84\, M_{min} - 0.19\, M_p - 0.18 \log M_0 + 7.4. \quad (5)$$

R and σ of Equation 5 are 0.56 and 0.28, respectively. The observed negative dependence between magnitude of the following main shock (M_f) and the magnitude of the preceding main shock (M_p) indicates that a large main shock is followed by a small one and vice versa.

Figure 4 (left panel) exhibits the frequency distribution of log (T/T_t) with a normal distribution (μ = 0) and having a standard deviation of σ = 0.32. The frequency distribution of the discrepancy between the observed (M_F) and the calculated (M_f) magnitudes which is compatible with μ = 0 and σ = 0.28 is shown in Figure 4 (right panel). A large scattering observed between the observed (T) and the calculated consecutive time interval (T_t) is clearly seen (Figure 4, left panel). Thus, it was assumed to obtain the probability of an event greater than a M_{min} (i.e. $M_{min} \geq 5.5$ for our case) and a certain time period. Considering log (T/T_t) in each zone, if there is an earthquake (M_p) occurred in t years before last observation date, the occurrence probability of a main shock ($M \geq M_{min}$) over the next Δt years can be obtained through the definition given below.

$$P(\Delta t) = P\left(L_1 \langle Z \langle L_2\right) = \frac{\left[F\left(\frac{L_2}{\sigma}\right) - F\left(\frac{L_1}{\sigma}\right)\right]}{\left[1 - F\left(\frac{L_1}{\sigma}\right)\right]} \quad (6)$$

where F represents the cumulative value of the normal distribution (μ = 0) and σ = 0.32, and

$$L_1 = log(t/T_t) \quad (7)$$
$$L_2 = log[\,(t+\Delta t)\,/\,T_t] \quad (8)$$

Table 3 shows the probabilities of a significant earthquake ($M_{min} \geq 7.0$) for the next 5 decades in the 7 seismogenic zones.

3.2. Earthquake building parameters for structural analysis

Generally, seismicity elements include some parameters such as fault and fault groups in the region, the

Table 1. Constants of each seismogenic zone, Gutenberg–Richter (1944) constants (*a* and *b*'), largest earthquake magnitude (M_{max}) and logarithm of moment ratio (log M_o).

Seismogenic zones		*a*	*b*'	M_{max}	log M_o
1	Kocaeli, Yalova	2.98	0.7	7.8	25.59
2	Bolu, Düzce, Sakarya	2.94	0.7	7.5	25.31
3	Çerkeş/Çankırı, Eskipazar/Karabük, Tosya/Kastamonu	5.00	0.9	7.2	25.42
4	Kargı/Çorum, Ladik/Samsun, Taşova/Amasya	4.00	0.9	7.0	24.70
5	Niksar/Tokat	4.00	0.9	7.1	24.76
6	Akıncılar/Sivas, Erzincan, Pülümür/Tunceli	3.30	0.7	7.9	25.95
7	Karlıova/Bingöl, Varto/Muş	6.00	0.9	6.9	25.87

Table 2. Earthquake data used for RTIMAP model; *a*: aftershocks, *f*: foreshocks, *M*: cumulative magnitude. The other terms are given in the text.

Seismogenic zones	Completeness Year	M_c	Date dd.mm.yy	Coordinates (°N)	(°E)	M_S	*M*	M_{min}	M_P	M_f	T_t (years)
Zone 1	1509	7.0	25.05.1719	40.70	29.50	7.0	7.0	5.5	7.0	7.0	35.27
	1900	5.5	02.09.1754	40.80	29.40	7.0	7.0	5.5	7.0	6.7	123.62
			19.04.1878	40.80	29.00	6.7	6.7	5.5	6.7	5.5	29.33
			21.08.1907	40.70	30.10	5.5	5.5	5.5	5.5	5.5	15.76
			29.05.1923	41.00	30.00	5.5	5.5	5.5	5.5	6.3	40.3
			18.09.1963	40.77	29.12	6.3	6.3	5.5	6.3	7.8	35.9
			17.08.1999	40.74	29.96	7.8	7.8	6.3	7.0	7.0	35.27
			13.09.1999	40.75	30.08	5.5	*a*	6.3	7.0	6.7	123.62
			20.09.1999	40.74	29.33	5.5	*a*	6.3	6.7	6.3	85.41
			11.11.1999	40.74	30.27	5.9	*a*	6.3	6.3	7.8	35.9
								6.7	7.0	7.0	35.27
								6.7	7.0	6.7	123.62
								6.7	6.7	7.8	121.32
								7.0	7.0	7.0	35.27
								7.0	7.0	7.8	244.95
Zone 2	1719	7.0	24.01.1928	40.99	30.86	5.5	5.5	5.5	5.5	6.7	14.98
	1900	5.5	20.01.1943	40.80	30.50	6.6	6.7	5.5	6.7	7.2	14.35
			20.06.1943	40.84	30.60	6.2	*a*	5.5	7.2	7.3	10.15
			05.04.1944	40.84	31.12	5.6	*a*	5.5	7.3	7.5	32.3
			26.05.1957	40.70	30.90	7.2	7.2	6.7	6.7	7.2	14.35
			26.05.1957	40.60	30.74	5.5	*a*	6.7	7.2	7.3	10.15
			26.05.1957	40.76	30.81	5.9	*a*	6.7	7.3	7.5	32.3
			27.05.1957	40.73	30.95	5.8	*a*	7.2	7.2	7.3	10.15
			22.07.1967	40.67	30.69	7.3	7.3	7.2	7.3	7.5	32.3
			22.07.1967	40.70	30.80	5.5	*a*	7.3	7.3	7.5	32.3
			30.07.1967	40.72	30.52	5.6	*a*				
			17.08.1999	40.64	30.65	5.6	*f*				
			06.09.1999	40.76	31.07	5.7	*f*				
			12.11.1999	40.81	31.19	7.5	7.5				
			12.11.1999	40.74	31.05	5.5	*a*				

Table 2. (Continued)

Seismogenic zones	Completeness Year	M_c	Date dd.mm.yy	Coordinates (°N)	(°E)	M_S	M	M_{min}	M_P	M_f	T_t (years)
Zone 3	968	7.0	25.06.1910	41.00	34.00	6.5	6.5	5.5	6.5	5.7	9.04
	1900	5.5	09.08.1918	40.89	33.41	5.8	*a*	5.5	5.7	5.5	17.44
			09.06.1919	41.16	33.20	5.7	5.7	5.5	5.5	7.5	7.02
			18.11.1936	41.25	33.33	5.5	5.5	5.5	7.5	5.7	33.89
			26.11.1943	41.05	33.72	7.2	7.5	5.5	5.7	5.7	22.66
			01.02.1944	41.41	32.69	7.2	*a*	5.7	6.5	5.7	9.04
			01.02.1944	41.40	32.70	5.5	*a*	5.7	5.7	7.5	24.46
			10.02.1944	41.00	32.30	5.5	*a*	5.7	7.5	5.7	33.89
			02.03.1945	41.20	33.40	5.6	*a*	5.7	5.7	5.7	22.66
			26.10.1945	41.54	33.29	5.7	*a*	6.5	6.5	7.5	33.41
			13.08.1951	40.88	32.87	6.9	*a*				
			07.09.1953	41.09	33.01	6.0	*a*				
			05.10.1977	41.02	33.57	5.7	5.7				
			06.06.2000	40.70	32.99	5.7	5.7				
Zone 4	1598	7.0	29.08.1918	40.58	35.16	5.5	5.5	5.5	5.5	7.0	24.3
	1900	5.5	21.11.1942	40.82	34.44	5.5	*f*	5.5	7.0	6.1	54.21
			02.12.1942	41.04	34.88	5.5	*f*	6.1	7.0	6.1	54.21
			11.12.1942	40.76	34.83	5.9	*f*				
			20.12.1942	40.66	36.35	7.0	7.0				
			10.12.1943	41.00	35.60	5.6	*a*				
			30.09.1944	41.11	34.87	5.5	*a*				
			10.08.1996	40.74	35.29	5.6	*f*				
			10.03.1997	40.78	35.44	6.0	6.1				
Zone 5	127	7.0	28.05.1914	39.84	35.80	5.5	*f*	6.3	7.1	6.3	24.84
	1900	5.5	24.01.1916	40.27	36.83	7.1	7.1				
			29.04.1923	40.07	36.43	5.9	*a*				
			28.12.1939	40.47	37.00	5.7	*f*				
			13.04.1940	40.04	35.20	5.6	*f*				
			30.07.1940	39.64	35.25	6.2	6.3				
			27.01.1941	39.68	35.31	5.7	*a*				
Zone 6	1890	7.0	16.02.1904	40.30	38.40	5.5	5.5	5.5	5.5	6.4	5.06
	1900	5.5	09.02.1909	40.00	38.00	6.3	6.4	-	6.4	6.3	20.27
			09.02.1909	40.00	38.00	5.8	*a*	-	6.3	7.9	10.6
			10.02.1909	40.00	38.00	5.7	*a*	-	7.9	5.9	20.83
			05.03.1909	39.70	40.50	5.5	*a*	-	5.9	6.3	6.74
			18.05.1929	40.20	37.90	6.1	6.3	-	6.3	6.3	24.61
			19.05.1929	40.02	37.90	6.1	*a*	-	6.3	6.2	10.86
			25.05.1929	40.02	37.90	5.5	*a*	-	6.2	5.5	7.64
			10.12.1930	39.71	39.24	5.6	*a*	5.9	6.4	6.3	20.27
			20.11.1939	39.82	39.71	5.9	*f*	-	6.3	7.9	10.6
			26.12.1939	39.80	39.51	7.9	7.9	-	7.9	5.9	20.83
			27.12.1939	39.99	38.14	5.5	*a*	-	5.9	6.3	6.74

Table 2. (Continued)

Seismogenic zones	Completeness Year	M_c	Date dd.mm.yy	Coordinates (°N)	(°E)	M_S	M	M_{min}	M_P	M_f	T_t (years)
			08.11.1941	39.70	39.70	5.5	*a*	-	6.3	6.3	24.61
			10.11.1941	39.74	39.43	5.9	*a*	-	6.3	6.2	10.86
			10.11.1941	39.74	39.50	6.0	*a*	6.2	6.4	6.3	20.27
			17.08.1949	39.60	40.60	5.5	*a*	-	6.3	7.9	10.6
			20.08.1949	39.57	40.62	7.0	*a*	-	7.9	6.3	27.59
			30.10.1960	40.19	38.75	5.9	5.9	-	6.3	6.3	24.61
			26.07.1967	39.54	40.38	5.9	*f*	-	6.3	6.2	10.86
			30.07.1967	39.54	40.38	6.2	6.3	6.3	6.4	6.3	20.27
			13.03.1992	39.71	39.63	6.1	6.3	-	6.3	7.9	10.6
			15.03.1992	39.53	39.93	5.8	*a*	-	7.9	6.3	27.59
			05.12.1995	39.43	40.11	5.7	*a*	-	6.3	6.3	24.61
			05.12.1995	39.48	40.32	5.5	*a*	6.4	6.4	7.9	30.87
			27.01.2003	39.46	39.77	6.2	6.2				
			22.09.2011	39.79	38.85	5.5	5.5				
Zone 7	1890	7.0	30.05.1946	39.29	41.21	5.7	5.7	5.5	5.7	5.5	7.82
	1900	5.5	28.03.1954	39.03	40.97	5.5	5.5	-	5.5	5.5	7.86
			12.02.1962	39.00	41.60	5.5	5.5	-	5.5	7.0	4.52
			30.08.1965	39.36	40.79	5.6	*f*	-	7.0	5.5	15.60
			10.03.1966	39.20	41.60	5.6	*f*	-	5.5	6.1	23.05
			19.08.1966	38.99	41.77	5.5	*f*	5.7	5.7	7.0	20.30
			20.08.1966	39.37	40.89	6.2	*f*	-	7.0	6.1	38.56
			20.08.1966	39.42	40.98	6.0	*f*	6.1	7.0	6.1	38.56
			20.08.1966	39.06	40.76	6.1	*f*				
			20.08.1966	39.17	41.56	6.9	7.0				
			10.09.1969	39.25	41.38	5.5	*a*				
			27.03.1982	39.23	41.90	5.5	5.5				
			12.03.2005	39.39	40.85	5.6	*f*				
			14.03.2005	39.35	40.88	5.7	6.1				
			23.03.2005	39.39	40.80	5.6	*a*				
			06.06.2005	39.37	40.92	5.6	*a*				
			10.12.2005	39.38	40.85	5.5	*a*				
			25.08.2007	39.26	41.04	5.5	*a*				

characteristics of the faults, the distance of the structure to the faults, the earthquake history of the region and the characteristics of the previous earthquakes. Additionally, local soil conditions affect the seismic behaviour of the buildings. Earthquake design spectra and other data that used for structural analysis can be obtained from mutual interaction between these parameters. Differences in design spectra significantly affect demands for displacement in structural analysis. Structures which do not meet the target displacement demands at high values are clearly distant from true values for damage estimates and building performance. It is essential to realize local soil conditions and seismicity characteristics of the region and make them usable in building design and evaluation. The obtained earthquake parameter values directly affect the calculations related to the structural analysis (Borcherdt,

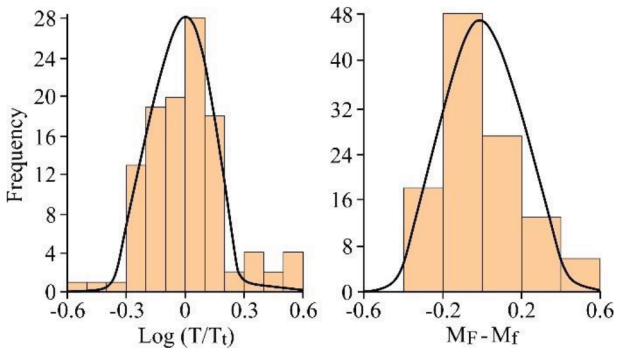

Figure 4. The frequency distribution of log (T/T_t) and the frequency distribution of M_F-M_f.

2004; Över et al., 2011; Büyüksaraç et al., 2013; Karaşin and Işık, 2017; Işık et al., 2016a, 2016b; Işık and Kutanis, 2015; Kutanis et al., 2018, Bekler et al., 2019).

Here, we examined the changes of the seismicity parameters for all selected settlements located on NAFZ (Figure 5). Four types of earthquake ground motion levels are identified in Turkish Seismic Design Code (TSDC-2019) (Table 4). Here, earthquake ground motion level DD-2 with a probability of exceedance 10% in 50 years (recurrence period 475 years) was selected for structural analysis. DD-2 was taken as standard design earthquake ground motion in TSDC-2019. Local soil class ZD type (Table 5) was selected to obtain horizontal and vertical elastic spectra. Short period map spectral acceleration coefficient (S_S), map spectral acceleration coefficient for the period of 1.0 s (S_1), PGA, local ground effect coefficients (F_S and F_1), design spectral acceleration coefficients (short period design spectral acceleration coefficient (S_{DS}), design spectral acceleration coefficients for 1.0 s period (S_{D1}), horizontal and vertical elastic design spectra were obtained from TEHMIWA for each settlement. The local soil effect coefficient F_S, local soil effect coefficient for 1.0 s period (F_1) for the ZD soil type with 5% damping ratio were calculated from Tables 6 and 7, respectively. Short period design spectral acceleration coefficient (S_{DS}) and S_{D1} were calculated using the following definitions:

$$S_{DS} = S_S \cdot F_S \quad (9)$$

$$S_{D1} = S_1 \cdot F_1 \quad (10)$$

Using the Turkish Earthquake Hazard Map that updated in 2019, seismic hazard analyses were performed to obtain PGA values for the different probabilities of exceedance. Table 8 clearly indicates that Bingöl/Karlıova and Muş/Varto are under the highest earthquake risk. Horizontal and vertical elastic design spectra obtained through TEHMIWA are illustrated in Figure 6. The sequences of S_S and S_1 values were obtained as the same order of PGA values. The S_S values for all settlements were determined between about 1.4–2.0 (Table 9). F_S coefficients are same for ZD soil type according to S_S given in Table 6. F_1 coefficients differ from each other according to S_1 values. Other earthquake parameters also vary depending on these values. The design spectra obtained in horizontal and vertical directions vary depending on the PGA values.

According to TSDC-2007 (TSDC-2007) and TBEC-2018 (TBEC-2018), the spectral acceleration coefficients and ground dominant periods of the design earthquake (DD-2) with a 10% probability of exceedance per 50 years are shown in Table 10. The spectral acceleration coefficient value is increased by approximately 96% in TBEC-2018, reaching the maximum level for Bingöl/Karlıova. It is increased by approximately 35% for the Düzce settlement which has the minimum value. The ground dominant periods, T_A and T_B, vary only depending on the soil classes in TSDC-2007. Since the same soil classes chosen for each settlement, T_A and T_B values are 0.15 and 0.60, respectively. These values are different from each other for each geographical location according to TBEC-2018.

Table 3. Probabilities of occurrence ($P_{\Delta t}$) for large ($M_{min} \geq 7.0$) earthquake for the next 5 decades in the 7 seismogenic zones and calculated magnitude values (M_f).

Seismogenic zones	M_f	T_t	P_{10}	P_{20}	P_{30}	P_{40}	P_{50}
	$M_{min} \geq 7.0$						
Zone 1	7.2	72.20	0.08	0.18	0.29	0.38	0.47
Zone 2	7.3	43.00	0.20	0.37	0.51	0.62	0.70
Zone 3	7.3	64.40	0.16	0.29	0.39	0.49	0.56
Zone 4	7.5	53.80	0.18	0.32	0.45	0.54	0.61
Zone 5	7.5	93.50	0.11	0.21	0.30	0.38	0.44
Zone 6	7.1	59.90	0.17	0.31	0.42	0.51	0.58
Zone 7	7.3	45.20	0.21	0.38	0.51	0.60	0.68

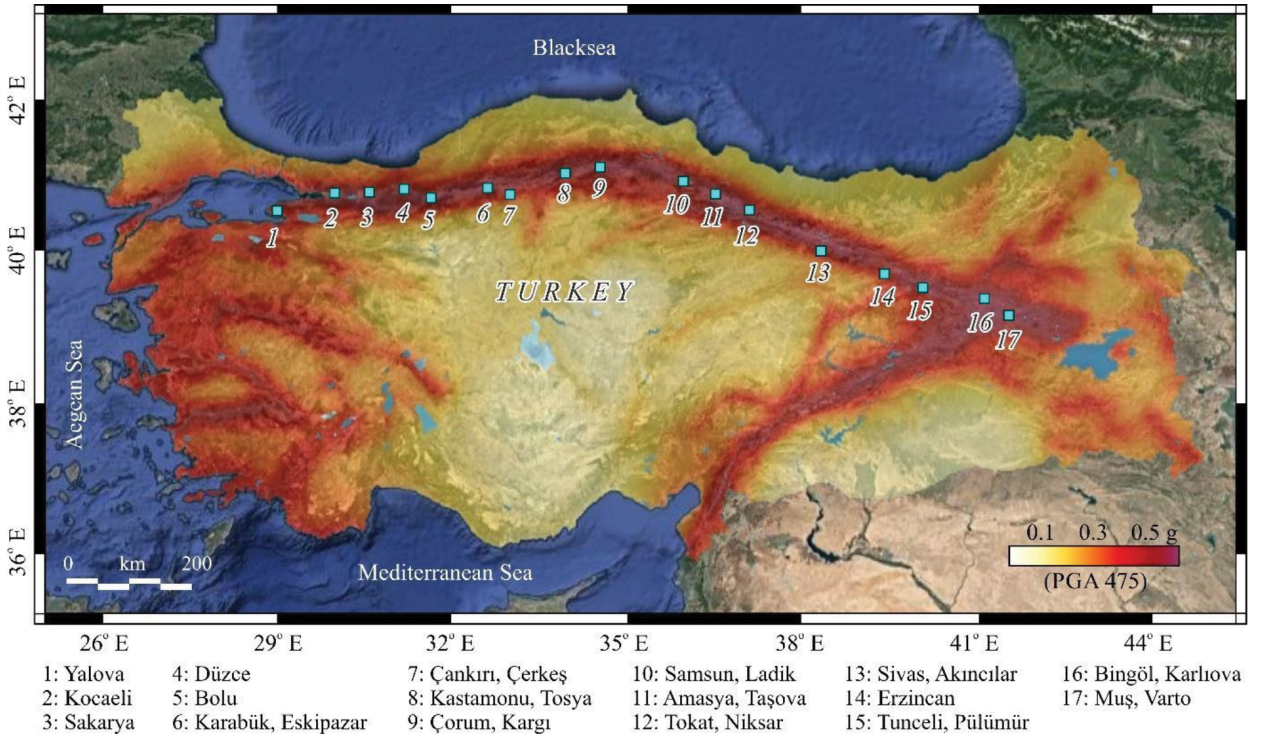

Figure 5. Seismic Hazard Map of Turkey and selected settlements.

Table 4. Earthquake ground motion levels (TSDC-2019).

Earthquake level	Repetition period	Probability of exceedance (in 50 years) (%)	Description
DD-1	2475	2	Largest earthquake ground motion
DD-2	475	10	Standard design earthquake ground motion
DD-3	72	50	Frequent earthquake ground motion
DD-4	43	68	Service earthquake movement

Table 5. The properties of ZD (TSDC-2019).

Local soil class	Type of soil	Average at the top 30 m		
		$(V_S)_{30}$ [m/s]	$(N_{60})_{30}$ [penetration/30 cm]	$(c_u)_{30}$ [kPa]
ZD	Medium tight - firm sand, gravel or very solid clay layers	180–360	15–50	70–250

Table 6. Local soil effect coefficients (F_S) for class ZD.

Local soil class	Local soil effect coefficient for the short period zone (F_S)					
	$S_S \leq 0.25$	$S_S = 0.50$	$S_S = 0.75$	$S_S = 1.00$	$S_S = 1.25$	$S_S \geq 1.50$
ZD	1.60	1.40	1.20	1.10	1.00	1.00

Table 7. Local ground effect coefficients for class ZD (F_1).

Local soil class	Local ground effect coefficient for 1.0 s period (F_1)					
	$S_1 \leq 0.10$	$S_1 = 0.20$	$S_1 = 0.30$	$S_1 = 0.40$	$S_1 = 0.50$	$S_1 \geq 0.60$
ZD	2.40	2.20	2.00	1.90	1.80	1.70

Table 8. PGA values obtained for different possibilities of exceedance for selected settlements.

Settlements	PGA (g)			
	Probability of exceedance in 50 Years			
	2%	10%	50%	68%
Akıncılar/Sivas	1.139	0.665	0.278	0.165
Bolu	1.078	0.629	0.241	0.139
Çerkeş/Çankırı	0.963	0.568	0.227	0.144
Düzce	0.924	0.553	0.196	0.113
Erzincan	1.101	0.597	0.216	0.147
Eskipazar/Karabük	1.084	0.686	0.243	0.152
Kargı/Çorum	1.146	0.670	0.295	0.173
Karlıova/Bingöl	1.339	0.792	0.353	0.201
Kocaeli	1.136	0.667	0.276	0.142
Ladik/Samsun	1.092	0.625	0.248	0.160
Niksar/Tokat	1.132	0.664	0.285	0.178
Pülümür/Tunceli	0.980	0.592	0.253	0.152
Sakarya	1.016	0.651	0.254	0.135
Taşova/Amasya	1.137	0.674	0.280	0.180
Tosya/Kastamonu	1.005	0.582	0.252	0.162
Varto/Muş	1.221	0.706	0.301	0.164
Yalova	0.957	0.598	0.232	0.144

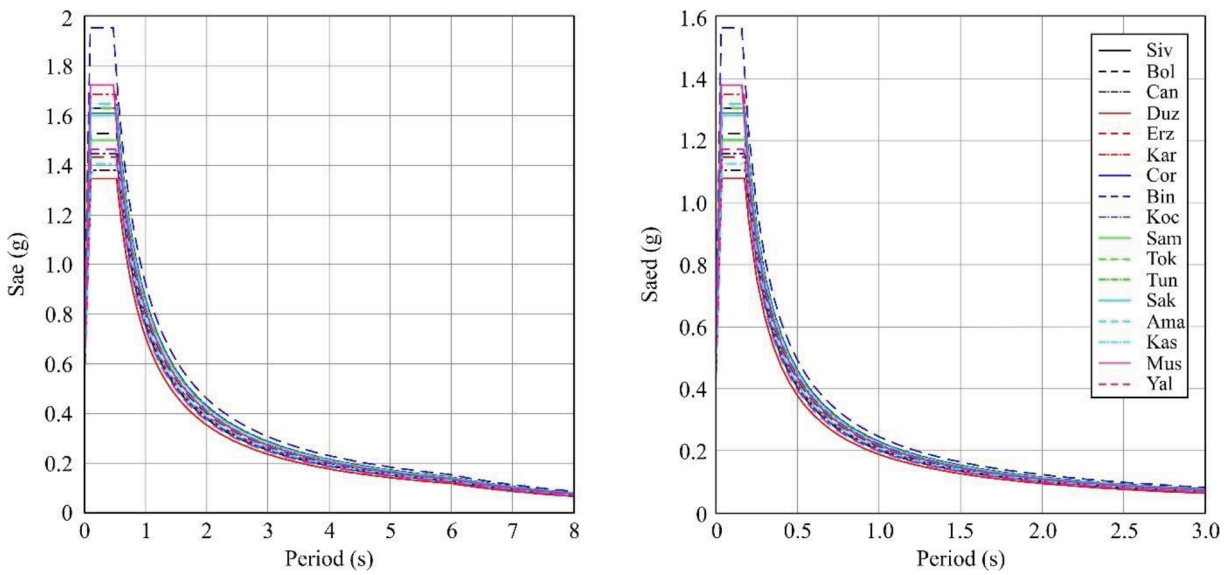

Figure 6. Horizontal (left panel) and vertical elastic design spectra (right panel) of the selected settlements.

Table 9. Comparison of earthquake parameters (DD-2 /ZD). T_A and T_B are the horizontal elastic design acceleration spectrum corner period (s), T_L is the transition period to fixed displacement zone in the horizontal elastic design spectrum (s), T_{AD} and T_{BD} represent the vertical elastic design acceleration spectrum corner period (s), and T_{LD} denotes the transition period to fixed displacement zone in the vertical elastic design spectrum (s). The other terms are given in the text.

Settlements	Earthquake parameters											
	S_S	S_1	F_S	F_1	S_{DS}	S_{D1}	T_A	T_B	T_L	T_{AD}	T_{BD}	T_{LD}
Akıncılar/Sivas	1.611	0.462	1.00	1.838	1.611	0.849	0.105	0.527	6.000	0.035	0.176	3.000
Bolu	1.528	0.429	1.00	1.871	1.528	0.803	0.105	0.525	6.000	0.035	0.175	3.000
Çerkeş/Çankırı	1.380	0.397	1.00	1.903	1.380	0.755	0.109	0.547	6.000	0.036	0.182	3.000
Düzce	1.347	0.365	1.00	1.935	1.347	0.906	0.105	0.524	6.000	0.035	0.175	3.000
Erzincan	1.434	0.413	1.00	1.887	1.434	0.779	0.109	0.543	6.000	0.036	0.181	3.000
Eskipazar/Karabük	1.686	0.472	1.00	1.828	1.686	0.863	0.102	0.512	6.000	0.034	0.171	3.000
Kargı/Çorum	1.631	0.469	1.00	1.831	1.631	0.859	0.105	0.527	6.000	0.035	0.176	3.000
Karlıova/Bingöl	1.955	0.516	1.00	1.955	1.955	0.921	0.094	0.471	6.000	0.031	0.157	3.000
Kocaeli	1.631	0.444	1.00	1.856	1.631	0.824	0.101	0.505	6.000	0.034	0.168	3.000
Ladik/Samsun	1.502	0.436	1.00	1.864	1.502	0.813	0.108	0.541	6.000	0.036	0.018	3.000
Niksar/Tokat	1.631	0.463	1.00	1.837	1.631	0.851	0.104	0.521	6.000	0.035	0.174	3.000
Pülümür/Tunceli	1.447	0.402	1.00	1.898	1.447	0.763	0.105	0.527	6.000	0.035	0.176	3.000
Sakarya	1.602	0.439	1.00	1.861	1.602	0.817	0.102	0.510	6.000	0.034	0.170	3.000
Taşova/Amasya	1.649	0.462	1.00	1.838	1.649	0.849	0.103	0.515	6.000	0.034	0.172	3.000
Tosya/Kastamonu	1.406	0.410	1.00	1.890	1.406	0.775	0.110	0.551	6.000	0.037	0.184	3.000
Varto/Muş	1.724	0.440	1.00	1.860	1.724	0.818	0.095	0.475	6.000	0.032	0.158	3.000
Yalova	1.465	0.389	1.00	1.911	1.465	0.743	0.101	0.507	6.000	0.034	0.169	3.000

Table 10. The comparison of spectral acceleration coefficients and ground dominant periods.

Settlements	TBEC-2018		TSDC-2007		TBEC-2018		TSDC-2007	
	S_{DS}	$0.40\ S_{Ds}$	S_{DS}	$0.40\ S_{Ds}$	T_A	T_B	T_A	T_B
Akıncılar/Sivas	1.611	0.644	1	0.40	0.105	0.527	0.15	0.60
Bolu	1.528	0.611			0.105	0.525		
Çerkeş/Çankırı	1.380	0.552			0.109	0.547		
Düzce	1.347	0.539			0.105	0.524		
Erzincan	1.434	0.574			0.109	0.543		
Eskipazar/Karabük	1.686	0.674			0.102	0.512		
Kargı/Çorum	1.631	0.652			0.105	0.527		
Karlıova/Bingöl	1.955	0.782			0.094	0.471		
Kocaeli	1.631	0.652			0.101	0.505		
Ladik/Samsun	1.502	0.601			0.108	0.541		
Niksar/Tokat	1.631	0.652			0.104	0.521		
Pülümür/Tunceli	1.447	0.579			0.105	0.527		
Sakarya	1.602	0.641			0.102	0.510		
Taşova/Amasya	1.649	0.660			0.103	0.515		
Tosya/Kastamonu	1.406	0.562			0.110	0.551		
Varto/Muş	1.724	0.690			0.095	0.475		
Yalova	1.465	0.586			0.101	0.507		

3.3. Structural analysis for sample RC building along the NAFZ

Structural analyses were carried out using academic licensed finite element package Seismostruct software (Seismosoft Inc., Pavia, Italy). The static adaptive pushover method in which the effect of the frequency content and deformation of the ground motion on the dynamic behaviour of the structure is considered to get the capacity of the structure under horizontal loads was performed in the analyses. In this method, analyses are carried out taking into account the mode shapes and participation factors determined from the eigenvalue analyses at each step. The method allows the use of site-specific spectra, especially where local soil conditions are considered. Load distributions and strain profiles can be obtained for the structure. In conventional pushover analysis, the input, functionality and load control types considered are similar to static adaptive pushover analysis (Antoniou and Pinho, 2003, 2004a, 2004b; Pinho and Antoniou, 2005; Casarotti and Pinho, 2007; Pinho et al., 2007, 2009; Ferracuti et al., 2009). A seven-story RC building with the same structural characteristics was chosen as an example to reveal the structural analysis results differences for the settlements on the fault zone. Calculations were performed in only one direction, since the RC building was chosen symmetrically in both directions. The blueprint of the selected RC building is shown in Figure 7.

Permanent and incremental loads were applied to the structure and incremental load values were selected as displacement. Permanent load value of 5.0 kN was considered and target displacement was selected as 0.2 m. These values were taken as the same in all models. Three-dimensional model obtained for the structure and the loads that were applied are given in Figure 8. Each story has an equal height of 3 m. The material class used for all load-bearing elements of the structure was selected as C25-S420. All columns and beams were selected as 0.40 m × 0.50 m and 0.25 m × 0.60 m, respectively. The transverse reinforcements used in both elements were set to ϕ10/10. The reinforcements used in the columns were set to 4ϕ20 at corners and 4ϕ16 top bottom and left-right sides. These values were selected to 4ϕ16 at lower side, 5ϕ14 upper side and 2ϕ12 at side for the beams. The columns and beams used for the structure are shown in Figure 9. The damping ratio was set to % 5 in all structural models. The ZD class was chosen as the ground class. The importance of structure was taken into consideration as Class III. The slabs were selected as rigid diaphragms.

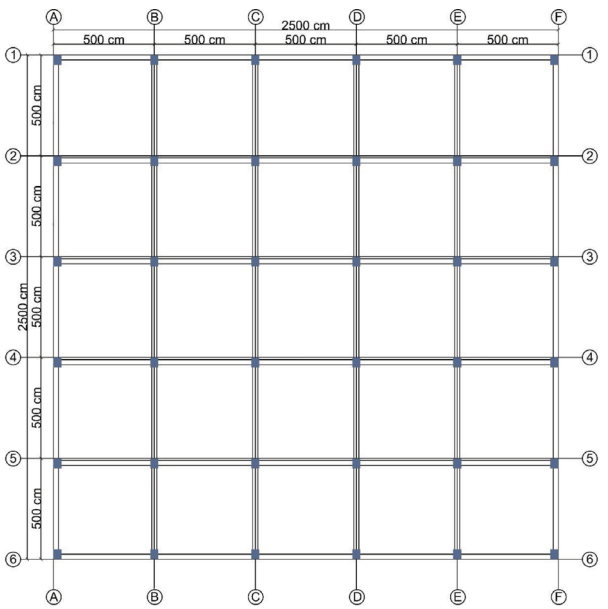

Figure 7. Floor formwork plan for the reinforced concrete structure selected as an example.

The structures are exposed to vibration movement under the effect of earthquake. These movements are a combination of harmonic modes. Mode shapes and natural frequency for any structure can be obtained by using eigenvalue analysis. Structure-related modal period, frequency, modal participation factors, effective modal masses and their percentages can be calculated by this analysis (Luo et al., 2017; Antoniou and Pinho, 2003; Kutanis et al., 2017; Nikoo et al., 2017). Based on the eigenvalue analysis the natural vibration period is 0.552 s for TSDC-2007 and 0.926 s for TBEC-2018. Additionally, TBEC-2018 suggests an analytical expression for the building natural vibration period (T_{PA}) as

$$T_{PA} = C_t \cdot H_N^{3/4} \tag{11}$$

where, H_N is the building total height; C_t is the correction coefficient. C_t takes four different values. If structural system formed by only columns and beams in RC building frames, $C_t = 0.1$, $C_t = 0.08$ for steel frames; $C_t = 0.07$ for all other buildings. According to the Equation 11, natural vibration period for 7-story building of 21 m height was found to be T = 0.981 s.

Rayleigh formula, which existed in TBEC-2018 and TSDC-2007, will continue to be used in the calculation of the natural vibration period of the structures. There is no such empirical formula in TSDC-2007. However, an update was made in TBEC-2018 by changing the empirical formula coefficient existing in TSDC-1998. Thus, in order to make comparison, we used this equation. The definition considered in TSDC-1998 is empirically calculated by Equation 11 for the fundamental period of vibration (T_{1A}). However, C_t coefficients take different values. It is taken as $C_t = 0.07$, since the structure chosen as an example here, consists only of RC frame. Therefore, the natural vibration

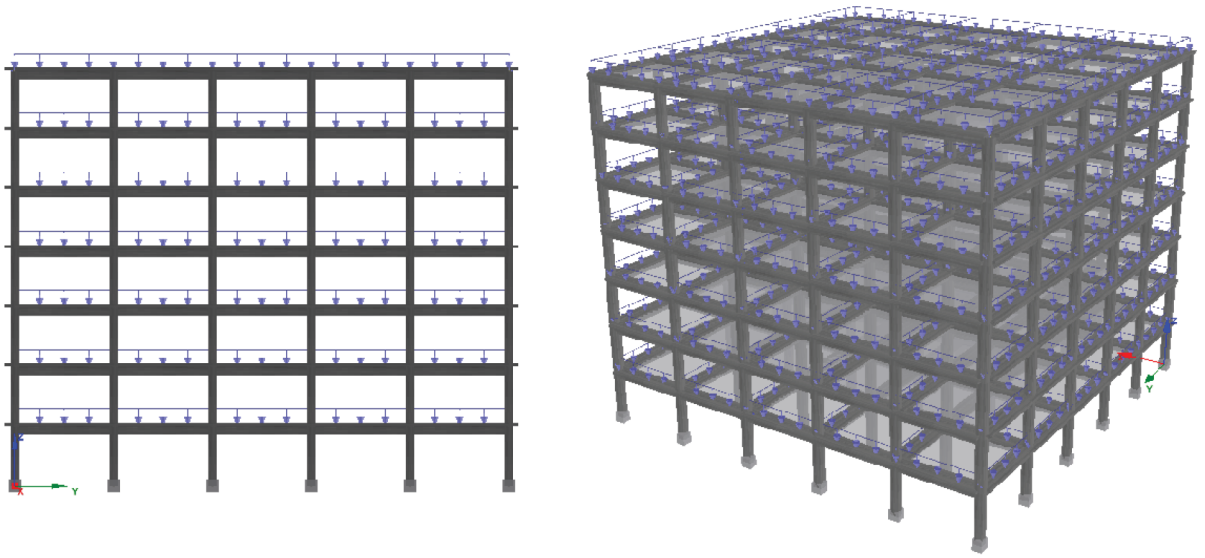

Figure 8. Three- and two-dimensional models of the selected BA structure.

period for the sample building was calculated as T = 0.687 s according to the previous regulation.

The sample RC building was analysed using the horizontal design spectrum curves and the base shear forces were calculated. The displacement values were obtained for three different points on the idealized curve. The first, second and third values refer to displacement at the moment of yield, to the intermediate (d_{int}) displacement and to the target displacement, respectively. Elastic stiffness (*K_elas*) and effective stiffness (*K_eff*) values were also calculated separately for all models. Three different performance criteria were obtained for damage estimation. These are considered as near collapse (*NC*), significant damage (*SD*) and damage limitation (*DL*). These values were calculated separately for all settlements. The comparison of all values obtained in x-direction is shown in Table 11. The comparison of the static pushover curves determined for the settlements are shown in Figure 10. The

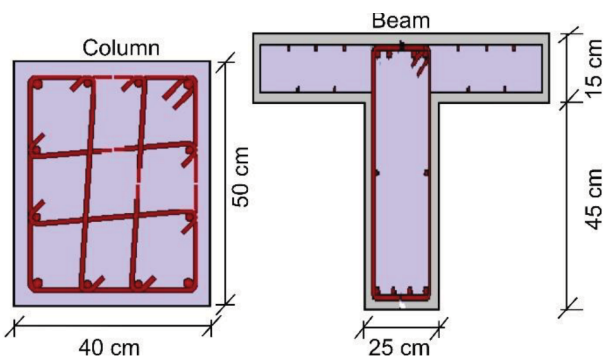

Figure 9. Column and beam cross sections.

design spectra significantly affected the performance levels expected from the structure. Significant changes were obtained in the target displacement demands foreseen for the earthquake performance level for damage estimation. Although there are no significant differences between the base shear forces, small differences were observed. Additionally, there were no significant differences in other structural analyses. Here, the PGA values calculated for the standard design earthquake ground motion for the probability of exceedance 10% were used which are given previously in Table 8. We determined that there is a complete agreement between PGA and displacement demands.

In order to compare the results obtained through the updated earthquake code with the previous one, Bingöl/Karlıova and Düzce settlements were selected since they produced the highest and the lowest PGA values, respectively. As the previous regulation does not include vertical design spectrum curves horizontal elastic design spectrums were used for the comparison. The comparison was made for the earthquake ground motion level using 10% probability of exceedance (repetition period 475 years) in 50 years since it is the only one in the previous code. A single spectrum curve is shown for TSDC-2007 for all settlements that considered in this study because of all these settlements were in the first-degree earthquake hazard zone. The horizontal elastic design spectrum curves foreseen for all settlements are different according to the previous regulation as clearly seen from Figure 11.

It was observed that updated spectrum curves are quite different from the previous spectrum curve for all settlements. This situation significantly changes the displacement

Table 11. Comparison of the values obtained in line X.

Settlements	Base shear (kN)	Displacement (m)	K_elas (kN/m)	K-eff (kN/m)	DL (m)	SD (m)	NC (m)
Akıncılar/Sivas	9161.51	0.1201	162508.30	76309.87	0.204	0.262	0.455
		0.2519					
		0.5303					
Bolu	9168.80	0.1211	162508.30	75720.33	0.194	0.248	0.432
		0.2521					
		0.5035					
Çerkeş/Çankırı	9143.52	0.1197	162508.30	76413.61	0.174	0.223	0.387
		0.2527					
		0.4526					
Düzce	9180.13	0.1212	162508.30	75732.94	0.170	0.219	0.379
		0.2597					
		0.4426					
Erzincan	9144.44	0.1198	162508.30	76351.90	0.183	0.235	0.408
		0.2598					
		0.4173					
Eskipazar/Karabük	9171.36	0.1209	162508.30	75839.03	0.211	0.271	0.470
		0.2525					
		0.4703					
Kargı/Çorum	9170.45	0.1211	162508.30	75718.87	0.207	0.265	0.460
		0.2521					
		0.4597					
Karlıova/Bingöl	9142.14	0.1196	162508.30	76448.24	0.243	0.312	0.541
		0.2614					
		0.5408					
Kocaeli	9145.95	0.1197	162508.30	76407.84	0.205	0.263	0.455
		0.2517					
		0.4556					
Lâdik/Samsun	9147.22	0.1197	162508.30	76401.38	0.192	0.246	0.427
		0.2525					
		0.4269					
Niksar/Tokat	9154.48	0.1198	162508.30	76407.06	0.204	0.262	0.454
		0.2451					
		0.4535					
Pülümür/Tunceli	9138.51	0.1198	162508.30	76313.03	0.182	0.233	0.405
		0.2627					
		0.4240					
Sakarya	9152.28	0.1200	162508.30	76293.44	0.200	0.257	0.445
		0.2531					
		0.4450					
Taşova/Amasya	9161.78	0.1203	162508.30	76140.21	0.207	0.266	0.461
		0.2849					
		0.4612					
Tosya/Kastamonu	9165.04	0.1206	162508.30	75998.74	0.180	0.230	0.399
		0.2510					
		0.4195					
Varto/Muş	9172.92	0.1208	162508.30	75920.63	0.218	0.280	0.484
		0.2518					
		0.4838					
Yalova	9153.46	0.1200	162508.30	76294.84	0.184	0.236	0.409
		0.2525					
		0.4217					

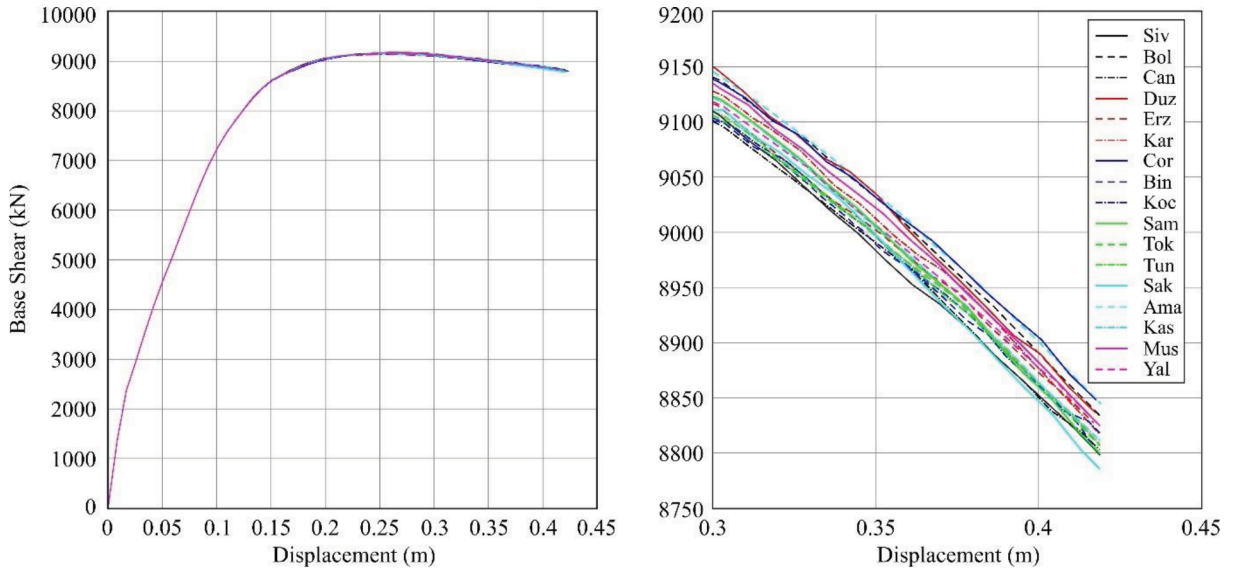

Figure 10. Static pushover curves obtained for the settlements.

demands. It is clear that damage estimates and building performance will diverge from real values in structures whose displacement demands are not met. The comparison of target displacements for damage estimation values obtained via the design spectrum for TSDC-2007 for sample RC building with the values obtained for the updated code is shown in Table 12. The analyses were carried out using same design spectrum curve for all settlements on the NAFZ, which are in the first-degree earthquake hazard zone in the previous regulation.

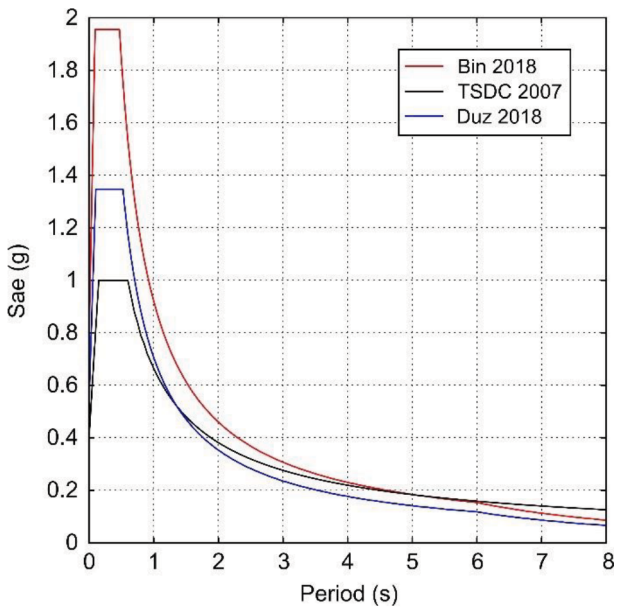

Figure 11. Comparison of the previous and updated horizontal design spectrum curves for the settlements having the highest and lowest PGA values.

Therefore, the values to be obtained take the same values for these provinces located in the same earthquake hazard zone. It was determined that the values obtained separately for each settlement are quite different from the previous one by using the site-specific design spectrum, which has been used with the updated regulation. Target displacements are higher than the values predicted in TSDC-2007 for all settlements. It is obvious that all the settlements which use the same design spectrum are insufficient according to TSDC-2007. This finding shows that the updates will yield more realistic displacement demands for the structures. Same target displacements were obtained for all settlements on the NAFZ located in the same earthquake hazard zone in the previous regulation. However, the values obtained through the updated regulation are different for all. This reveals the necessity of site-specific design spectrum instead of regional-based design spectrum that was used in TSDC-2007.

4. Discussion and conclusion

The lithology and segmentation of fault planes can be important control actors on seismic slip propagation. Coulomb stress reveals an interactive earthquake triggering cycle between two adjacent normal and strike-slip faults. Static Coulomb stress variation can be calculated to investigate the triggering effect of an earthquake on nearby subsequent events and after shocks. Also, a static Coulomb stress increase greater than 0.01 MPa can have significant triggering effects (Zhang et al. 2008). Considering the NAFZ in two parts as the east and west sections would be a correct distinction especially in terms of stress accumulations. There was a marked accumulation of high stress in the eastern part of the NAFZ and subsequent

Table 12. Comparison of target displacements for damage estimation according to previous and updated codes.

Settlements	Code	Target displacement (m)		
		DL	*SD*	*NC*
All settlements	TSDC-2007	0.052	0.076	0.155
Karlıova/Bingöl	TBEC-2018	0.243	0.312	0.541
Varto/Muş		0.218	0.280	0.484
Eskipazar/Karabük		0.211	0.271	0.470
Taşova/Amasya		0.207	0.266	0.461
Kargı/Çorum		0.207	0.265	0.460
Kocaeli		0.205	0.263	0.455
Akıncılar/Sivas		0.204	0.262	0.455
Niksar/Tokat		0.204	0.262	0.454
Sakarya		0.200	0.257	0.445
Bolu		0.194	0.246	0.427
Ladik/Samsun		0.192	0.246	0.427
Yalova		0.184	0.236	0.409
Erzincan		0.183	0.235	0.408
Pülümür/Tunceli		0.182	0.233	0.405
Tosya/Kastamonu		0.180	0.230	0.399
Çerkeş/Çankırı		0.174	0.223	0.387
Düzce		0.170	0.219	0.379

stress transfer between 1939 and 1944. However, since the stress accumulation in the western part is longer, the time interval between the occurrence periods of earthquakes are wider. The proximity to the tectonic source may have been effective in this case.

It is well-known that time depended seismicity models for earthquake occurrences in seismogenic zones are of great importance to perform seismic hazard assessment. Thus, we applied RTIMAP model and predicted the likelihood probabilities of subsequent events and magnitudes within 5 decades in the predefined 7 seismogenic zones on NAFZ which is one of the main structures controlling the neotectonics of Turkey. Generally, the probability of earthquake occurrences in these zones is considerably high. We determined that a large earthquake event ($M_S \geq 7.0$) in the next 50 years (2020–2070) may most likely (P_{50} = 70 %) occur in the zone 2. The magnitude and repetition time of the next large event for this zone 2 were determined as M_f = 7.3 and T_t = 43 years, respectively. The final occurrence used in the determination of the probability of a large event in this zone was occurred in 1999 (M_S = 7.5). The other high probability for $M_S \geq 7.0$ in 50 years was determined as P_{50} = 68% for the seismogenic zone 7. M_f = 7.3 and T_t = 45.2 years were computed for this zone. The earthquake occurred in 1966 (M_S = 7.0) was used to determine the probability. In addition to the region-based RTIMAP model studies, we also performed point-based site-specific seismic hazard analyses for 17 different settlements located along the NAFZ according to different probabilities of exceedance in 50 years. We determined that Bingöl/Karlıova and Muş/Varto are under the highest earthquake risk. This finding supports the RTIMAP model which produced high probability of earthquake occurrence for zone 2. However, some discrepancies between the results due to the nature of these approaches were obtained. It must be also noted that instrumental ($M_S \geq 5.5$, until the end of 2019) and historical earthquakes with maximum intensities of $I_0 \geq 9.0$ corresponding to surface wave magnitude $M_S \geq 7.0$ were used in the RTIMAP model while all the past events were used in the point-based site-specific seismic hazard analyses.

In addition to seismicity parameters and hazard analyses, structural parameters were also obtained for 17 settlements. Understanding the hazard analyses obtained regionally and determining the vulnerability

levels of similar structures in different areas of hazard are important in terms of establishing the relationship between earthquake hazard and building behaviour. We determined the differences in seismic performance values of sample RC building with similar structural characteristics along the fault zone. Horizontal and vertical elastic spectra curves used to express earthquake effects in buildings were obtained and remarkable differences were observed. This finding is due to the seismicity elements of the settlements, fault/fault groups and their properties, the distance of the geographical locations to the fault/fault groups, the earthquake history of the region. This indicates that obtaining design spectra by using the site-specific earthquake hazard based on updated TSDC-2018 is a significant gain. The natural vibration period values determined according to the latest regulation are higher than those of the previous regulation. Therefore, it is expected that the structures behave more ductile with the latest regulation. Static adaptive pushover analysis performed for the sample RC building using the design spectra obtained for each settlement showed that site-specific design spectra directly affect building performance under earthquake impact. The 2007 seismic code states the earthquake regions. In this code, the effective ground acceleration coefficient for first degree regions is 0.40 g while it is 0.30 g for second degree regions. However, values obtained for the updated 2019 code indicates higher values. Thus, we mentioned that the structural performance analyses for earthquake resistant structural design can be determined more accurately via point basis site-specific studies instead of regional basis studies.

Conflict of interest

The authors declare that there is no conflict of interest.

References

Al-Tarazia E, Sandvol E (2007). Alternative models of seismic hazard evaluation along the Jordan-Dead Sea transform. Earthquake Spectra 23: 1-19.

Ambraseys NN (1970). Some characteristic features of the North Anatolian Fault zone. Tectonophysics 9: 43-165.

Antoniou S, Pinho R (2003). Seismostruct–seismic analysis program by Seismosoft. User Manual. Pavia, Italy: Seismosoft Inc.

Antoniou S, Pinho R (2004a). Advantages and limitations of force-based adaptive and non-adaptive pushover procedures. Journal of Earthquake Engineering 8: 497-522.

Antoniou S, Pinho R (2004b). Development and verification of a displacement-based adaptive pushover procedure. Journal of Earthquake Engineering 8: 643-661.

Barka AA (1992). The North Anatolian fault. Annales Tectonic 6: 64-195.

Bayliss TJ, Burton PW (2007). A new earthquake catalogue for Bulgaria and the conterminous Balkan high hazard region. Natural Hazards Earth System Science 7: 45-359.

Bekler T, Demirci A, Ekinci YL, Büyüksaraç A (2019). Analysis of localsite conditions through geophysical parameters at a city under earthquake threat: Çanakkale, NW Turkey. Journal of Applied Geophysics 163: 31-39.

Bektaş O, Eyüboğlu Y, Maden N (2007). Different modes of stress transfer in a strike-slip fault zone: an example from the North Anatolian Fault System in Turkey. Turkish Journal of Earth Sciences 16: 1-12.

Borcherdt RD (2004). A theoretical model for site coefficients in building code provisions. In: Proceedings of 13th World Conference on Earthquake Engineering; Vancouver, BC, Canada. pp. 1-6.

Bozkurt E (2001). Neotectonics of Turkey–a synthesis. Geodinamica Acta 14: 3-30.

Burton PW, Xu Y, Qin C, Tselentis GA (2004). A catalogue of seismicity in Greece and the adjacent areas for the twentieth century. Tectonophysics 390: 117-127.

Büyüksaraç A, Bektaş Ö, Yılmaz H, Arısoy MÖ (2013). Preliminary seismic microzonation of Sivas city (Turkey) using microtremor and refraction microtremor (ReMi) measurements. Journal of Seismology 17: 425-435.

Caputo M (1974). Analysis of seismic risk. Nato Advanced Study Institutes Series. Applied Sciences 3. Leiden, Netherlands: Noordhoff International Publishing.

Casarotti C, Pinho R (2007). An adaptive capacity spectrum method for assessment of bridges subjected to earthquake action. Bulletin of Earthquake Engineering 5: 377-390.

Chingtham P, Yadav RBS, Chopra S, Yadav AK, Gupta AK et al. (2016). Time-dependent seismicity analysis in the Northwest Himalaya and its adjoining regions. Natural Hazards 80: 1783-1800.

Coral A (2006). Dependence of earthquake recurrence times and independence of magnitudes on seismicity history. Tectonophysics 424: 177-193.

Cornell CA (1968). Engineering seismic risk analysis. Bulletin of the Seismological Society of America 58: 1583-1606.

Dewey JF (1976). Seismicity of northern Anatolia. Bulletin of the Seismological Society of America 66: 843-868.

Ekinci YL, Büyüksaraç A, Bektaş Ö, Ertekin C (2020). Geophysical investigation of Mount Nemrut Stratovolcano (Bitlis, Eastern Turkey) through aeromagnetic anomaly analyses. Pure and Applied Geophysics 172 (7): 3243-3264.

Ekinci YL, Balkaya Ç, Göktürkler G, Özyalın Ş (2021). Gravity data inversion for the basement relief delineation through global optimization: a case study from the Aegean Graben System, Western Anatolia, Turkey. Geophysical Journal International 224 (2): 923-944.

Ferracuti B, Pinho R, Savoia M, Francia R (2009). Verification of displacement-based adaptive pushover through multi-ground motion incremental dynamic analyses. Engineering Structures 31: 1789-1799.

Gutenberg B, Richter CF (1944). Frequency of Earthquakes in California. Bulletin of the Seismological Society of America 34: 185-188.

Hamling IJ, D'Anastasio E, Wallace LM, Ellis S, Motagh M et al. (2014). Crustal deformation and stress transfer during a propagating earthquake sequence: The 2013 Cook Strait sequence, central New Zealand. Journal of Geophysical Research: Solid Earth 119 (7): 6080-6092.

Harris RA, Simpson RW (1996). In the Shadow of 1857—The effect of the great ft. tejon earthquake on subsequent earthquakes in Southern California. Geophysical Research Letters 23 (3): 229-232.

Hubert-Ferrari A, Armijo R, King G, Meyer B, Barka A (2002). Morphology, displacement, and slip rates along the North Anatolian Fault, Turkey. Journal of Geophysical Research-Solid Earth 107: 2235.

Işık E, Kutanis M, Bal İE (2016a). Displacement of the buildings according to site-specific earthquake spectra. Periodica Polytechnica Civil Engineering 60: 37-43.

Işık E, Büyüksaraç A, Aydin MC (2016b). Effects of local soil conditions on earthquake damages. In: Górecki J (editor). Journal of Current Construction Issues. Civil Engineering Present Problems, Innovative Solutions - Sustainable Development in Construction. BGJ Consulting, Bydgoszcz, Poland pp. 191-198.

Işık E, Kutanis M (2015). Determination of local site-specific spectra using probabilistic seismic hazard analysis for Bitlis Province, Turkey. Earth Sciences Research Journal 19: 129-134.

Işık E, Büyüksaraç A, Ekinci YL, Aydın MC, Harirchian E (2020). The effect of site-specific design spectrum on earthquake-building parameters: a case study from the Marmara Region (NW) Turkey. Applied Sciences 10 (20): 7247.

İşseven T, Tüysüz O (2006). Paleomagnetically defined rotations of fault-bounded continental blocks in the North Anatolian Shear Zone, North Central Anatolia. Journal of Asian Earth Sciences 28: 469-479.

Karaşin İB, Işık E (2017). Farklı yapı davranış katsayıları için zemin koşullarının yapı performansına etkisi. DÜMF Mühendislik Dergisi 8: 661-673.

King GCP, Stein RS, Lin J (1994). Static stress changes and the triggering of earthquakes. Bulletin of Seismological Society of America 84: 935-953.

Kutanis M, Ulutaş H, Işik E (2018). PSHA of Van province for performance assessment using spectrally matched strong ground motion records. Journal of Earth System Science 127: 99.

Kutanis, M, Boru EO, Işık E (2017). Alternative instrumentation schemes for the structural identification of the reinforced concrete field test structure by ambient vibration measurements. KSCE Journal of Civil Engineering 21: 1793-1801.

Luo YF, Liu YP, Hu ZY, Xiong Z (2017). A new method for dynamic analysis of spatial lattice structures based on mode selection and mode construction techniques. International Journal of Steel Structures 17: 1157-1170.

Makropoulos K, Kaviris G, Kouskouna V (2012). An updated and extended earthquake catalogue for Greece and adjacent areas since 1900. Natural Hazards Earth System Science 12: 1425-1430.

McKenzie D (1972). Active tectonics of the Mediterranean region. Geophysical Journal Royal Astronomical Society 30: 109-185.

Mogi K (1985). Earthquake Prediction. Cambridge, MA, USA: Academic Press.

Molnar P (1979). Earthquake recurrence intervals and plate tectonics. Bulletin of the Seismological Society of America 69: 115-133.

Mulargia F, Geller RJ (2003). Earthquake science and seismic risk reduction. Dordrecht, Netherlands: Kluwer Academic Publishers.

Nikoo M, Hadzima-Nyarko M, Khademi F, Mohasseb S (2017) Estimation of fundamental period of reinforced concrete shear wall buildings using self-organization feature map. Structural Engineering and Mechanics 63: 237-249.

Okay AI, Tüysüz O (1999). Tethyan sutures of northern Turkey, in The Mediterranean Basins: Tertiary extension within the Alpine orogen, vol. 156, pp. 475–515, eds. Durand B, Jolivet L, Horvath F, Seranne M. Geological Society of London.

Över S, Büyüksaraç A, Bektaş Ö, Filazi A (2011). Assessment of potential seismic hazard and site effect in Antakya (Hatay Province), SE Turkey. Environmental Earth Sciences 62: 313-326.

Papadopoulos GA, Voidomatis P (1987). Evidence for periodic seismicity in the inner Aegean seismic zone. Pure and Applied Geophysics 125: 613-628.

Papazachos BC (1992). A time and magnitude-predictable model for generation of shallow earthquakes in the Aegean Area. Pure and Applied Geophysics 138: 287-308.

Papazachos BC, Papaioannou ChA (1993). Long-term earthquake prediction in the Aegean Area based on a time and magnitude predictable model. Pure and Applied Geophysics 140: 593-612.

Papazachos BC, Papadimitriou EE, Karakaisis GF, Panagiotopoulos DG (1997). Long-term earthquake prediction in the circum-Pacific convergent belt. Pure and Applied Geophysics 149: 173-217.

Papazachos BC, Karakaisis GF, Scordilis EM (2014). Time dependent seismicity in the continental fracture system. Bollettino di Geofisica Teorica e Applicata 55: 617-639.

Papazachos BC, Karakaisis GF, Scordilis EM, Papaioannou ChA (2016). Seismogenic sources in the Aegean area and their predictive properties. Bulletin of the Geological Society of Greece L: 1222-1231.

Parsons T, Toda S, Stein RS (2000). Heightened odds of large earthquakes near Istanbul: an interaction-based probability calculation. Science 288: 661-665.

Paudyal H, Singh HN, Shanker D, Singh VP (2008). Validity of time-predictable seismicity model for Nepal and its adjoining regions. Journal of Nepal Geological Society 38: 15-22.

Pinho R, Casarotti C, Antoniou S (2007). A Comparison of single-run pushover analysis techniques for seismic assessment of bridges. Earthquake Engineering and Structural Dynamics 36: 1347-1362.

Pinho R, Monteiro R, Casarotti C, Delgado R (2009). Assessment of continuous span bridges through nonlinear static procedures. Earthquake Spectra 25: 143-159.

Pinho R, Antoniou S (2005). A Displacement-based adaptive pushover algorithm for assessment of vertically irregular frames. In: Proceedings of the Fourth European Workshop on the Seismic Behaviour of Irregular and Complex Structures; Thessaloniki, Greece.

Sayil N (2013). Long-term earthquake prediction in western Anatolia with the time- and magnitude-predictable model. Natural Hazards 66: 809-834.

Sayil N (2014). Evaluation of the seismicity for the Marmara region with statistical approaches. Acta Geodetica Geophysica 49: 265-281.

Shanker D, Panthi A, Singh HN (2012). Long-term seismic hazard analysis in Northeast Himalaya and its adjoining regions. Geosciences Journal 2: 25-32.

Shanker D (1990). Characteristic studies of tectonics, Seismicity and occurrences of major earthquakes in northeast India. PhD, Banaras Hindu University, Varanasi, India.

Shebalin NV, Leydecker G, Mokrushina NG, Tatevossian RE, Erteleva OO et al. (1998). Earthquake catalogue for central and southeastern Europe 342BC-1990AD. Final report ETNU-CT93-0087. Brussels, Belgium: European Commission.

Stein RS, Barka AA, Dietrich JH (1997). Progressive failure on the north Anatolian fault since 1939 by earthquake stress triggering. Geophysical Journal International 128: 594-604.

Sengor AMC (1979). The north Anatolian transform fault: Its age offset and tectonic significance. Journal of the Geological Society of London 136: 269-282.

Şengör AMC, Görür N, Şaroğlu F (1985). Strike-slip faulting and related basin formation in zones of tectonic escape: Turkey as a case study. In: Biddle KT, Christie-Slick N (editors). Strike-slip Faulting and Basin Formation. Society of Economic Paleontologist and Mineralogists 37: 227-264.

Şengör AMC, Tüysüz O, İmren C, Sakınç M, Eyidoğan H et al. (2005). The North Anatolian Fault Zone: a new look. Annual Review of Earth and Planetary Sciences 33: 37-112.

Şengör AMC, Grall C, İmren C, Le Pichon X, Görür N et al. (2014). The geometry of the North Anatolian transform fault in the Sea of Marmara and its temporal evolution: implications for the development of intracontinental transform faults. Canadian Journal of Earth Sciences 51: 222-242.

TSDC- 1998, Turkish Seismic Design Code.

TSDC- 2007, Turkish Seismic Design Code.

TBEC-2018, Turkish Building Earthquake Code. T.C. Resmi Gazete; 30364.

Tatar O, Piper JDA, Park RG, Gürsoy H (1995). Palaeomagnetic study of block rotations in the Niksar overlap region of the North Anatolian Fault Zone, central Turkey. Tectonophysics 244: 251-266.

Tatar O, Piper JDA, Gürsoy H, Temiz H (1996). Regional significance of neotectonic counterclockwise rotation in Central Turkey. International Geology Review 38: 692-700.

Tatar O, Poyraz F, Gürsoy H, Cakir Z, Ergintav S et al. (2012). Crustal deformation and kinematics of the Eastern part of the North Anatolian Fault Zone (Turkey) from GPS measurements. Tectonophysics 518-521: 55-62.

Weisberg S (1980). Applied Linear Regression. Hoboken, NJ, USA: Wiley-Interscience.

Yiğitbaş E, Elmas A, Sefunç A, Özer N (2004). Major neotectonic features of eastern Marmara region, Turkey: Development of the Adapazari-Karasu corridor and its tectonic significance. Geological Journal 39: 179-198.

Zabcı C (2019). Spatio-temporal behaviour of continental transform faults: implications from the late Quaternary slip history of the North Anatolian Fault, Turkey. Canadian Journal of Earth Sciences 56: 1218-1238.

Zhang Z, Chen J YS, Lin J (2008). Stress interactions between normal faults and adjacent strike-slip faults of 1997 Jiashi earthquake swarm. Science in China Series D: Earth Sciences 51 (3): 431-440.